# Properties of H particle-admixed compact star

Xuhao Wu<sup>1</sup>, Liming Wang <sup>1,4</sup>,\* Hong-Tao An<sup>2,3,4</sup>,<sup>†</sup> Min Ju<sup>5</sup>,<sup>‡</sup> and Hong Shen<sup>6</sup>§

<sup>1</sup>Key Laboratory for Microstructural Material Physics of Hebei Province,
School of Science, Yanshan University, Qinhuangdao 066004, China

<sup>2</sup>School of Physical Science and Technology, Lanzhou University, Lanzhou 730000, China

<sup>3</sup>Research Center for Hadron and CSR Physics, Lanzhou University
and Institute of Modern Physics of CAS, Lanzhou 730000, China

<sup>4</sup>Lanzhou Center for Theoretical Physics, Key Laboratory of Theoretical Physics of Gansu Province,
and Frontiers Science Center for Rare Isotopes, Lanzhou University, Lanzhou 730000, China

<sup>5</sup>School of Science, China University of Petroleum (East China), Qingdao 266580, China

<sup>6</sup>School of Physics, Nankai University, Tianjin, 300071, China

We explore the potential manifestation of a hexaquark, the H particle, as a constituent within neutron stars. The H particle, characterized by a quark composition of uuddss, is constructed using the framework of Chromomagnetic Interaction (CMI). Specifically, we contemplate the flavor-singlet state H with  $J^P = 0^+$ . Our computations indicate that the three-flavor hexaquark state, the H particle, possesses a lower mass of 2212.7 MeV in comparison to the  $d^*(2380)$ , implying greater stability than the two-flavor  $d^*(2380)$ . The analysis involving the H particle is carried out using the relativistic mean-field (RMF) model. We investigate the influence of H particle couplings, a key factor in determining the system stability, and focus on the potential existence of H particle within neutron stars. We find that H particle could potentially endure as a stable constituent within neutron stars, and lead to a reduction of the maximum mass.

#### I. INTRODUCTION

In 1977, Jaffe [1] proposed a stable H particle which has quark composition uuddss. This proposal was based on a perturbative bag model together with a bound state formed by two  $\Lambda$ 's. The H particle is a spin-0, flavor-singlet, parity-even boson with electric charge Q=0, baryon number B=2 and strangeness number S=-2, which should be the most tightly-bound state of hexaquark (also known as sexaquarks). It is interesting to explore the possibility that H particle could exist in neutron star (NS) core.

Traditionally, the core of NS has been modeled as a uniform fluid composed of neutron-rich nuclear matter in  $\beta$  equilibrium. However, at the extremely high densities in NS core, it is expected that new degrees of freedom will emerge beyond nucleons [2]. The candidates can include hyperons [3–9],  $\Delta$ -isobars [8–13], di-baryonic matter [13–17] and deconfined quark matter [18–24]. The presence of these exotic degrees of freedom in NSs are generally in competition with other constitutes, affecting all particles' fraction, softening the equation of state (EOS), and reducing the maximum mass of the NS. The existence of the dibaryon in NSs is possible under high chemical potentials, and its bosonic nature sets it apart from the normal fermionic constituents such as nucleons and leptons. Extensive studies have been conducted on the hexaquark  $d^*(2380)$  [25–27], supported by experi-

\*Electronic address: lmwang@ysu.edu.cn †Electronic address: anht14@lzu.edu.cn ‡Electronic address: jumin@upc.edu.cn §Electronic address: shennankai@gmail.com mental evidence [28].  $d^*(2380)$  shares the same composition of u, d quarks and does not involve any strangeness degrees of freedom. Despite its large mass,  $d^*(2380)$  still can exist in the interior of NSs [13]. At high densities, three flavor quark matter may be more stable than two flavor quark matter [29, 30]. The H particle, possessing three-flavor symmetry, is expected to be more stable than  $d^*(2380)$  with lower mass and energy per baryon, making it capable of stably existing in the core of NSs.

In recent years, significant progresses have been made in observing and obtaining information about the properties of NS, such as mass, radius and tidal deformability. A noteworthy event is the observation of the most accurate massive NS, PSR J0740+6620 [31, 32], which has a lower limit of  $2.14^{+0.10}_{-0.09}~M_{\odot}$  (68.3% credibility interval). This measurement rules out those EOS which predict NS maximum mass  $(M_{\text{max}})$  lower than this value. Another remarkable discovery is the heaviest NS known as PSR J0952-0607, which reports a mass of  $2.35 \pm 0.17~M_{\odot}$  [33] (68.3% credibility inter-Additional observations of massive NS include the accurate mass determination of object like PSR  $J1614-2230 (1.908\pm0.016M_{\odot})$  [34] and PSR J0348+0432 $(2.01\pm0.04M_{\odot})$  [35]. The simultaneous measurements on mass and radius of PSR J0030+0451 from the Neutron Star Interior Composition Explorer (NICER) give the range (68% credible interval)  $M = 1.34^{+0.15}_{-0.16} M_{\odot}, R =$  $12.71_{-1.19}^{+1.14}$  km [36] as well as  $M = 1.44_{-0.14}^{+0.15}$   $M_{\odot}$ , R = $13.02_{-1.06}^{+1.24}$  km [37]. Similar measurements from NICER for PSR J0740+6620 provide the results (68.3% credibility interval)  $M = 2.072^{+0.067}_{-0.066} M_{\odot}, R = 12.39^{+1.30}_{-0.98} \text{ km [38]}$ and  $M = 2.08 \pm 0.07 M_{\odot}$ ,  $R = 13.7^{+2.6}_{-1.5}$  km [39]. The binary NS merger event GW170817 provided a constraint on the tidal deformability of a canonical 1.4  $M_{\odot}$  NS with  $\Lambda_{1.4} < 800$  [40]. Furthermore, the inferred constraint on

 $R_{1.4}$  from GW170817 indicates  $R_{1.4} < 13.6$  km [41]. In another gravitational wave event, the secondary component of GW190814 with a mass of  $2.5 \sim 2.67 M_{\odot}$  [42] could potentially be a NS. In this case, the corresponding constraint on tidal deformability reads  $458 \leq \Lambda_{1.4} \leq 889$  [42].

In the present work, we aim to investigate the impact of a new degree of freedom in NS matter, namely the H particle. We explore the possible coupling strengths of H particle as a free parameter for the effective interaction within the relativistic mean-field (RMF) model. We treat the isovector coupling by two methods: (1) using a constant isovector coupling referred to as RMF model; and (2) using a density-dependent isovector coupling referred to as RMFL model. Furthermore, we analyze the effects of H particle on the properties of NS.

The manuscript is organized in the following way. The Chromomagnetic Interaction (CMI) framework is presented in Section II to calculate the mass of H particle. In Section III we describe NS matter containing H particle using RMF/RMFL models. Our main results concerning the appearance and effects of H particle on NSs are shown and discussed in Section IV Finally, the conclusions are provided at the end of the manuscript in Section V.

#### II. MASS SPECTRUM OF nnnnss STATE

# A. Effective Hamiltonian and corresponding parameters

For the ground mass of nnnnss (I=0) states, we consider the chromomagnetic interaction model [43–46]. Here, n quark in nnnnss states represents u or d quark. The corresponding effective Hamiltonian is

$$H = \sum_{i} m_{i}^{0} + H_{\text{CEI}} + H_{\text{CMI}}$$

$$= \sum_{i} m_{i}^{0} - \sum_{i < j} A_{ij} \vec{\lambda}_{i} \cdot \vec{\lambda}_{j} - \sum_{i < j} v_{ij} \vec{\lambda}_{i} \cdot \vec{\lambda}_{j} \vec{\sigma}_{i} \cdot \vec{\sigma}_{j},$$

$$= -\frac{3}{4} \left( -\frac{4}{3} \sum_{i} m_{i}^{0} \right) - \sum_{i < j} A_{ij} \vec{\lambda}_{i} \cdot \vec{\lambda}_{j}$$

$$- \sum_{i < j} v_{ij} \vec{\lambda}_{i} \cdot \vec{\lambda}_{j} \vec{\sigma}_{i} \cdot \vec{\sigma}_{j},$$

$$= -\frac{3}{4} \sum_{i < j} \left[ \frac{1}{4} (m_{i}^{0} + m_{j}^{0}) + \frac{4}{3} A_{ij} \right] \vec{\lambda}_{i} \cdot \vec{\lambda}_{j}$$

$$- \sum_{i < j} v_{ij} \vec{\lambda}_{i} \cdot \vec{\lambda}_{j} \vec{\sigma}_{i} \cdot \vec{\sigma}_{j},$$

$$= -\frac{3}{4} \sum_{i < j} m_{ij} V_{ij}^{C} - \sum_{i < j} v_{ij} V_{ij}^{CMI}.$$
(1)

In the above expression,  $V_{ij}^{\rm C} = \vec{\lambda}_i \cdot \vec{\lambda}_j$  and  $V_{ij}^{\rm CMI} = \vec{\lambda}_i \cdot \vec{\lambda}_j \vec{\sigma}_i \cdot \vec{\sigma}_j$  denote the color and color-magnetic interactions between quarks, respectively.  $\sigma_i$  is the Pauli matrix and  $\lambda_i$  is the Gell-Mann matrix.

TABLE I: Coupling parameters of the nnnnss states (in units of MeV)

$m_{nn}$	$m_{ns}$	$m_{ss}$	$v_{nn}$	$v_{ns}$	$v_{ss}$
181.2	226.7	262.3	19.1	13.3	12.2

The  $m_{ij}$  is a mass parameter of quark pair:

$$m_{ij} = \frac{1}{4}(m_i^0 + m_j^0) + \frac{4}{3}A_{ij}, \tag{2}$$

which mainly determine the size of the mass. And, the  $v_{ij}$  is the effective coupling constant between the *i*-th quark and *j*-th quark, which mainly determine the mass gaps. It depends on the quark masses and the ground particle's spatial wave function. The parameters  $m_{ij}$  and  $v_{ij}$  are extracted from the traditional hadron masses [43]. Here, we present the coupling parameters about nnnss states in Table I.

#### B. Wave Functions

In order to calculate the mass spectrum of nnnnss (I=0) states, we also need to construct the total wave function satisfied with Pauli Principle. The total wave function of nnnnss (I=0) states is described by the direct product of space, flavor, color, and spin wave functions

$$\psi_{\text{tot}} = \psi_{space} \otimes \psi_{flavor} \otimes \psi_{color} \otimes \psi_{spin}. \tag{3}$$

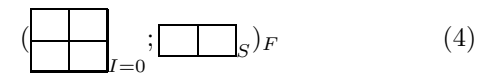
Here, we only consider the low-lying S-wave dibaryon states since the symmetrical constraint from spatial dibaryon wave function is trivial. Thus, others should be fully antisymmetric when exchanging identical quarks. For nnnnss (I=0) states, we need to construct  $\psi_{flavor} \otimes \psi_{color} \otimes \psi_{spin}$  wave functions satisfied with  $\{1234\}\{56\}$  symmetry. Here, we use the notation  $\{1234\}$   $(\{56\})$  to label that the quark 1, 2, 3, and 4 (5 and 6) have antisymmetry property. Similarly, we also use the notation [1234] ([56]) to label that the quark 1, 2, 3, and 4 (5 and 6) have symmetry property.

Moreover, Young tableau, which represents the irreducible bases of the permutation group, enable us to easily identify the dibaryon configuration with certain symmetry property [47–49]. Therefore, we could use the Young tableau and the Young-Yamanouchi basis vector to describe the wave functions.

# 1. Flavor part

For the flavor part of the nnnnss (I=0) states, we consider SU(2) flavor symmetry and take the s quark as flavor singlet since the mass of s quark is much heavier

than the mass of n quark. Corresponding Young diagram of the nnnnss (I=0) states are shown in:



Based on this Young diagram, we obtain the corresponding Young tableau:

$$(\frac{12}{34}_{I-0}; \underline{56}_{S})_{F}; \quad (\frac{13}{24}_{I-0}; \underline{56}_{S})_{F}.$$
 (5)

2. Color part

For the color part, we only need to consider the color singlets based on the color confinement. Here, the color part is satisfied with the SU(3) symmetry. We can construct five color singlets and use corresponding Young tableau to represent them:

According to these five Young tableaux, we can obtain corresponding Young diagram:

Based on above Young diagram, we split it in the manner of [1234], [56] and get :

$$( \qquad ; \qquad ), \qquad ( \qquad ; \qquad ).$$
 (8)

3. Spin part

The spin part are based on the SU(2) symmetry. For nnnss states, all possible total spin are J=3,2,1, and 0, respectively. Here, we show corresponding Young tableaux for different spin states:

According to above twenty Young tableaux, we can obtain four corresponding Young diagram:



4.  $Flavor \otimes Color \otimes Spin part$ 

In order to satisfied with the  $\{1234\}\{56\}$  symmetry, we can get the Yang diagram of color  $\otimes$  spin part from the Yang diagram of flavor part:

$$( \longrightarrow_{I=0} ; \bigcirc_{S})_{F} \Rightarrow ( \longrightarrow_{S} ; \bigcirc_{CS}.$$
 (11)

For color  $\otimes$  spin part, it is satisfied with SU(6) symmetry. Here, we can take reduction SU(6)<sub>CS</sub>  $\supset$  SU(3)<sub>C</sub>  $\otimes$  SU(2)<sub>S</sub>:

We easily find that these three Young diagrams about color part are just correspond to the Young diagram of Eq.(8). Further, the first Young diagram about spin part corresponds to a J=2 state. Similarly, the second (third) Young diagram about spin part corresponds to a J=0 state (a J=0 state, a J=1 state, and a J=2 state). Other Young diagrams about color part can not form the color singlets, thus we do not need to consider it. Based on above discussions, there are two J=2 states, one J=1 state, and two J=0 states for ground nnnss (J=0) states.

By using the Clebsch-Gordan (CG) coefficient of the permutation group  $S_n$ , one obtains the coupling scheme designed to construct the the color  $\otimes$  spin wave functions. The expression of Clebsch-Gordan (CG) coefficient of  $S_n$  reads as [50]

$$S([f']p'q'y'[f'']p''q''y''|[f]pqy) = K([f']p'[f'']p''|[f]p)S([f'_{n'}]q'y'[f''_{n''}]q''y''|[f_p]qy).$$

$$(13)$$

Here, S in the left-hand (right-hand) side denotes a CG coefficient of  $S_n$  ( $S_{n-1}$ ) and the [f] ( $[f_p]$ ) is a Young tableau of  $S_n$  ( $S_{n-1}$ ) with [f]pqy as a specific Young-Yamanouchi basis vector. And, p (q) is the row of the n (n-1)-th particle in the Young-Yamanouchi basis vector, while y is the distribution of the n-2 remaining particles.

Based on these, we obtain the corresponding Young-Yamanouchi basis vector which are obtained form Eq. (12):

$$(\frac{1}{2}; \frac{5}{6})_{FCS} = \sqrt{\frac{1}{2}} (\frac{1}{3}; \frac{1}{4}; \frac{1}{5}; \frac{1}{6})_F \otimes (\frac{1}{3}; \frac{1}{5}; \frac{1}{6})_{CS} - \sqrt{\frac{1}{2}} (\frac{1}{3}; \frac{1}{3}; \frac{1}{5}; \frac{1}{5}; \frac{1}{6})_F \otimes (\frac{1}{3}; \frac{1}{5}; \frac{1}{6})_{CS}.$$
 (14)

$$\begin{pmatrix}
\boxed{1 \ 3} \\
\boxed{2 \ 4}
\end{pmatrix}; 
\begin{pmatrix}
\boxed{5} \\
\boxed{6}
\end{pmatrix}; 
C_S = -\sqrt{\frac{1}{2}} \frac{\boxed{1 \ 2}}{\boxed{3 \ 4}} \otimes \boxed{\frac{1 \ 3 \ 5}{2 \ 4 \ 6}}_{S_{20}} - \sqrt{\frac{1}{2}} \frac{\boxed{1 \ 3}}{\boxed{5 \ 6}}_{C_2} \otimes \boxed{\frac{1 \ 2 \ 5}{3 \ 4 \ 6}}_{S_{18}}.$$
(16)

$$\left(\begin{array}{c|c}
\hline{1 & 3} \\
\hline{2 & 4}
\end{array}\right)_{CS} = -\sqrt{\frac{2}{5}} \frac{\boxed{1} & 3}{5} \otimes \boxed{\frac{1}{5}} \frac{2 & 3 & 4 & 6}{5} & -\sqrt{\frac{1}{6}} \frac{\boxed{1} & 3}{2 & 5} \\
\hline{5} & S_3 & -\sqrt{\frac{1}{6}} \frac{\boxed{1} & 3}{4 & 6} & \otimes \boxed{\frac{1}{2}} \frac{3 & 4 & 5 & 6}{2} \\
\hline{2} & S_6
\end{array}.$$
(18)

$$J^{P} = 2^{+} : (\boxed{\frac{1}{3}} \boxed{\frac{2}{3}}, \boxed{\frac{5}{6}})_{CS} = -\sqrt{\frac{1}{3}} \boxed{\frac{1}{3}} \boxed{\frac{4}{5}} \otimes \boxed{\frac{1}{2}} \boxed{\frac{2}{5}} \boxed{\frac{5}{4}} \bigcirc -\sqrt{\frac{1}{6}} \boxed{\frac{1}{2}} \boxed{\frac{2}{5}} \bigcirc -\sqrt{\frac{1}{6}} \boxed{\frac{1}{2}} \boxed{\frac{2}{5}} \bigcirc -\sqrt{\frac{1}{6}} \boxed{\frac{1}{2}} \boxed{\frac{2}{5}} \bigcirc -\sqrt{\frac{1}{6}} \boxed{\frac{1}{2}} \bigcirc -\sqrt{\frac{1}{6}} \bigcirc -$$

$$-\sqrt{\frac{1}{3}}\frac{\frac{1}{3}\frac{2}{5}}{\frac{4}{6}}_{C_{1}} \otimes \frac{12356}{4}_{S_{4}}; \tag{19}$$

$$\frac{1}{2} \frac{3}{4}; \frac{5}{6} c_{S} = \sqrt{\frac{1}{3}} \frac{1}{\frac{1}{3}} \frac{4}{\frac{1}{3}} \otimes \frac{1}{3} \frac{1}{\frac{1}{3}} \frac{1}{\frac{1}{3}} \otimes \frac{1}{\frac{1}{3}} \frac{1}{\frac{1}{3}} \frac{1}{\frac{1}{3}} \frac{1}{\frac{1}{3}} \otimes \frac{1}{\frac{1}{3}} \frac{1}{\frac{1}{3}} \frac{1}{\frac{1}{3}} \otimes \frac{1}{\frac{1}{3}} \frac{1}{\frac{1}{3}} \frac{1}{\frac{1}{3}} \otimes \frac{1}{\frac{1}{3}} \frac{1}{\frac{1}$$

$$J^{P} = 0^{+} : (\frac{12}{34}, \frac{15}{6}) c_{S} = -\sqrt{\frac{1}{3}} \frac{114}{25} \\ \frac{12}{36} \\ \frac{1}{6} \\ \frac{1}{3} \\ \frac$$

# C. Numerical results

The mass spectra of nnnnss (I = 0) state is shown in Table II, in which  $J^P = 0^+$  state has  $m_H = m_{uuddss} = 2212.7$  MeV.

TABLE II: The mass of the nnnss (I=0) states (in units of MeV).

$J^P$	0+		1+	2+	
Mass	2569.4	2212.7	2360.1	2752.3	2458.8

# III. THE RMF/RMFL MODEL

The RMF/RMFL model is constructed based on the meson-exchange picture which describes the nucleon-nucleon (NN) interaction. In this model, the scalar  $(\sigma)$ 

meson represents the attractive component, while the vector meson  $(\omega)$  represents the repulsive component of the NN interaction. Additionally, the isovector meson  $(\rho)$ is introduced to account for the isospin difference between neutron (n) and proton (p). In this work, we focus on the properties of the H particle ( $m_H = 2212.7 \text{ MeV}$ ), which consists of the *uuddss* quarks, including strangeness degree. For simplicity, we do not consider the contribution of hidden-strangeness mesons  $(\sigma^*, \phi)$  here, which describe attractive and repulsive interactions involving strangeness. Instead, we employ the free couplings of  $g_{\sigma H}$  and  $g_{\omega H}$  to characterize the attractive and repulsive interactions of the H particle. By doing so, we effectively account for the effects of strangeness mesons within our model. It is worth noting that information regarding the H particle matter system is limited, and there is currently no consensus on the magnitude of the H particle potential. Therefore, adopting this approach allows us to reduce the number of free parameters in our study.

We utilize the RMF/RMFL model as our theoretical framework. The total Lagrangian consisting of nucleons,

leptons, mesons and H particles is given by

$$\mathcal{L}_{RMFL} = \mathcal{L}_{N} + \mathcal{L}_{l} + \mathcal{L}_{m} + \mathcal{L}_{H}, \qquad (25)$$

where

$$\mathcal{L}_{N} = \sum_{i=p,n} \bar{\psi}_{i} \left\{ i \gamma_{\mu} \partial^{\mu} - M^{*} - \gamma_{\mu} \left[ g_{\omega} \omega^{\mu} + \frac{g_{\rho}}{2} \tau_{a} \rho^{a\mu} \right] \right\} \psi_{i},$$
 (26)

$$\mathcal{L}_{l} = \sum_{l=e,\mu} \bar{\psi}_{l} \left( i \gamma_{\mu} \partial^{\mu} - m_{l} \right) \psi_{l}, \tag{27}$$

$$\mathcal{L}_{m} = \frac{1}{2} \partial_{\mu} \sigma \partial^{\mu} \sigma - \frac{1}{2} m_{\sigma}^{2} \sigma^{2} - \frac{1}{3} g_{2} \sigma^{3} - \frac{1}{4} g_{3} \sigma^{4}$$

$$- \frac{1}{4} W_{\mu\nu} W^{\mu\nu} + \frac{1}{2} m_{\omega}^{2} \omega_{\mu} \omega^{\mu} + \frac{1}{4} c_{3} (\omega_{\mu} \omega^{\mu})^{2}$$

$$- \frac{1}{4} R_{\mu\nu}^{a} R^{a\mu\nu} + \frac{1}{2} m_{\rho}^{2} \rho_{\mu}^{a} \rho^{a\mu}$$

$$+ \Lambda_{v} g_{\omega}^{2} g_{\rho}^{2} \omega_{\mu} \omega^{\mu} \rho_{\mu}^{a} \rho^{a\mu}, \qquad (28)$$

$$\mathcal{L}_{H} = (\partial_{\mu} - ig_{\omega H}\omega_{\mu}) \dot{\phi}_{H}^{*} (\partial^{\mu} + ig_{\omega H}\omega^{\mu}) \phi_{H}$$
$$- (m_{H} + g_{\sigma H}\sigma)^{2} \phi_{H}^{*} \phi_{H}, \tag{29}$$

with  $M^* = M + g_{\sigma}\sigma$  representing the effective mass of the nucleon. In the context of homogeneous nuclear matter, the meson field equation takes the following forms,

$$m_{\sigma}^{2}\sigma + g_{2}\sigma^{2} + g_{3}\sigma^{3} = -g_{\sigma} \left( n_{p}^{s} + n_{n}^{s} \right) - g_{\sigma H}n_{H}, \quad (30)$$
  

$$m_{\omega}^{2}\omega + c_{3}\omega^{3} + 2\Lambda_{v}g_{\omega}^{2}g_{\rho}^{2}\rho^{2}\omega = g_{\omega} \left( n_{p} + n_{n} \right) + g_{\omega H}n_{H}, \quad (31)$$

$$m_{\rho}^{2}\rho + 2\Lambda_{\rm v}g_{\omega}^{2}g_{\rho}^{2}\omega^{2}\rho = \frac{g_{\rho}}{2}\left(n_{p} - n_{n}\right),\tag{32}$$

where  $n_i^s$  and  $n_i$  (i=n,p) represent the scalar density and vector density, respectively. The isovector coupling  $g_{\rho}$  in RMFL is treated as a density-dependent function, following the approach used in the density-dependent RMF (DDRMF) framework,

$$g_{\rho}(n_b) = g_{\rho}(n_0) \exp\left[-a_{\rho} \left(\frac{n_b}{n_0} - 1\right)\right], \qquad (33)$$

where  $n_0$  is the saturation density. The density dependence of  $g_{\rho}$  contributes a rearrangement term for the nucleon vector potential,

$$\Sigma_r = \frac{1}{2} \sum_{i=p,n} \frac{\partial g_{\rho}(n_b)}{\partial n_b} \tau_3 n_i \rho = -\frac{1}{2} a_{\rho} g_{\rho}(n_b) \frac{n_p - n_n}{n_0} \rho.$$
(34)

The chemical potential of proton, neutron, leptons, and H particle are given by

$$\mu_p = \sqrt{(k_F^p)^2 + {M^*}^2} + g_\omega \omega + \Sigma_r + \frac{g_\rho(n_b)}{2} \rho, (35)$$

$$\mu_n = \sqrt{(k_F^n)^2 + M^{*2}} + g_\omega \omega + \Sigma_r - \frac{g_\rho(n_b)}{2} \rho,$$
 (36)

$$\mu_H = m_H + g_{\sigma H}\sigma + g_{\omega H}\omega, \tag{37}$$

$$\mu_l = \sqrt{k_{F_l}^2 + m_l^2}, \ (l = e, \mu).$$
 (38)

The  $\beta$  equilibrium condition in NS requires

$$\mu_n = \mu_p + \mu_e, \tag{39}$$

$$\mu_{\mu} = \mu_{e}, \tag{40}$$

$$\mu_H = 2\mu_n. \tag{41}$$

In the H particle admixed NS matter, the total pressure and energy density are given by

$$P = \sum_{i=p,n} \frac{1}{3\pi^2} \int_0^{k_F^i} \frac{1}{\sqrt{k^2 + M^{*2}}} k^4 dk$$

$$-\frac{1}{2} m_\sigma^2 \sigma^2 - \frac{1}{3} g_2 \sigma^3 - \frac{1}{4} g_3 \sigma^4 + \frac{1}{2} m_\omega^2 \omega^2$$

$$+\frac{1}{4} c_3 \omega^4 + \frac{1}{2} m_\rho^2 \rho^2 + n_b \Sigma_r + \Lambda_v g_\omega^2 g_\rho^2 \omega^2 \rho^2$$

$$+ \sum_{l=e,\mu} \frac{1}{3\pi^2} \int_0^{k_F^i} \frac{k^4 dk}{\sqrt{k^2 + m_l^2}}, \qquad (42)$$

$$\varepsilon = \sum_{b=n,p} \frac{1}{\pi^2} \int_0^{k_{F_b}} \sqrt{k^2 + m_b^{*2}} k^2 dk$$

$$+\frac{1}{2} m_\sigma^2 \sigma^2 + \frac{1}{3} g_2 \sigma^3 + \frac{1}{4} g_3 \sigma^4 + \frac{1}{2} m_\omega^2 \omega^2$$

$$+\frac{3}{4} c_3 \omega^4 + \frac{1}{2} m_\rho^2 \rho^2 + 3 \Lambda_v g_\omega^2 g_\rho^2 \omega^2 \rho^2 + m_H^* n_H$$

$$+ \sum_{l=e,\mu} \frac{1}{\pi^2} \int_0^{k_F^l} \sqrt{k^2 + m_l^2} k^2 dk \qquad (43)$$

When  $a_{\rho} = 0$ , the rearrangement term  $\Sigma_r$  vanishes. As a result, the isovector coupling  $g_{\rho}$  becomes a constant, and the RMFL model reduces to a general RMF model.

We note that H particle does not directly contribute to the pressure in NS matter. However, by affecting the strength of meson field, the presence of H particle can still influence the total pressure of the system. We apply four different parameter sets for the meson couplings, BigApple [51], NL3L-50 [52], TM1e [53, 54] and NL3 [55], which are listed in Table III. The existence of massive NSs requires a stiff EOS at the core. However, constraints of the tidal deformability and supernova explosion mechanism favor a soft normal neutron star crust. Among the parameter sets used in this study, BigApple, NL3L-50 and TM1e satisfy the maximum mass and tidal deformability requirements based on observation constraints. The NL3 parameter set is included as a comparison. The couplings between H particle and mesons are taken as free parameters in this study. In contrast to the choice made in Ref. [13], we consider only positive values for the dimensionless couplings  $\chi_{\sigma H} = g_{\sigma H}/g_{\sigma}$  and  $\chi_{\omega H} = g_{\omega H}/g_{\omega}$ . For example, with  $\chi_{\sigma H} = 0$ , a purely repulsive interaction similar to the negative values in Ref. [13] is formed. The same applies to  $\chi_{\omega H} = 0$  for the case of a purely attractive interaction. As we lack information of H particle potential, we explore a wide range for  $\chi_{\sigma H}$  and  $\chi_{\omega H}$  to determine the appropriate scale. In Ref. [13], the increasing fraction of  $d^*(2380)$  leads to an increase in the fraction of electrons, which contributes to the pressure. However, unlike  $d^*(2380)$ , the charge-neutral H particle does not have such an effect on electron fraction. Therefore, the presence of the H particle has a more pronounced impact on reducing the pressure compared to  $d^*(2380)$ . Usually a positive contribution of H particle to the pressure is favored when introducing a new degree of freedom at high densities in NS matter. In our study, we focus on the constraints derived from observations and entertain the possibility of H particle existing in a stable NS.

TABLE III: Masses of nucleons and mesons and meson coupling constants. The masses are given in MeV.

Parameters	BigApple	NL3L-50	TM1e	NL3
M	939.0	939.0	938.0	939.0
$m_{\sigma}$	492.730	508.194	511.198	508.194
$m_{\omega}$	782.500	782.501	783.000	782.501
$m_ ho$	763.0	763.0	770.0	763.0
$g_{\sigma}$	9.6699	10.217	10.0289	10.217
$g_{\omega}$	12.316	12.868	12.6139	12.868
$g_{ ho}(n_0)$	14.1618	8.948	12.2413	8.948
$g_2/{\rm fm}^{-1}$	11.9214	10.431	7.2325	10.431
$g_3$	-31.6796	-28.885	0.6183	-28.885
$g_{\omega 3}$	2.6843	0	71.3075	0
$\Lambda_v$	0.0475	0	0.0327	0
$a_{ ho}$	0	0.5835	0	0

# IV. RESULTS AND DISCUSSIONS

In Fig. 1, we show the onset density of the H particle as a function of the dimensionless couplings  $\chi_{\sigma H}$  and  $\chi_{\omega H}$ within NS matter. The nucleon component of the system is described using the BigApple, NL3L-50, TM1e, and NL3 parameter sets, respectively. In the case of purely attractive interaction ( $\chi_{\omega H} = 0$ ), the onset density of H particle decreases with  $\chi_{\sigma H}$  increases. Conversely, with a purely repulsive interaction ( $\chi_{\sigma H} = 0$ ), the appearance of H particle is delayed to higher densities for larger values of  $\chi_{\omega H}$ . When both  $\chi_{\sigma H}$  and  $\chi_{\omega H}$  are non-zero, the onset density could be connected to purely attractive case or purely repulsive case through the contour lines. The NL3L-50, BigApple and NL3 parameter sets yield similar results for the onset density. Comparing these with the results obtained using the relatively softer EOS TM1e, we find that the model dependence primarily stems from the stiffness of the EOS but have little dependence on the symmetry energy. With stiffer EOS, the onset density of H particle is smaller.

The stability of NS containing H particle is displayed in Fig. 2. The light blue region, labeled with the corresponding coupling strengths  $\chi_{\sigma H}$  and  $\chi_{\omega H}$  (step size 0.1), indicates a decrease in pressure upon the appearance of H particle. In other words, the presence of the H particle with the couplings of the blue region leads to an instability in the many-body system which may result in collapse of NS. The blue solid line represents the bound-

ary of the unstable region. The Yukawa potential can be defined according to Ref. [14], which requires

$$\frac{g_{\sigma H}^2}{m_{\sigma}^2} < \frac{g_{\omega H}^2}{m_{\omega}^2}.\tag{44}$$

The boundary where H particle does not contribute to the pressure, namely  $U_{\rm Yukawa}=\frac{g_{\sigma H}^2}{m_{\sigma}^2}-\frac{g_{\omega H}^2}{m_{\omega}^2}=0$ , is presented by the red solid line. There is a noticeable gap between the red and blue lines, indicating that despite the negative contribution from H particle, the strong repulsive interaction at high density and the Fermi degeneracy pressure from nucleons and leptons are able to sustain a stable system. However, this stability does not persist at higher densities, even with  $U_{\text{Yukawa}} > 0$  (located in the upper left of the red line), because the pressure provided by H particle is too small compared to other particles, and its fraction increases with density. On one hand, the fractions of nucleons and leptons decrease, which lead to a reduction of their contributions to the pressure. On the other hand, H particle contributes only a minimal amount of pressure, even if it has a positive value, but it cannot balance the reduction from other particles. There is a extreme case that H particle could exhibit a total repulsive interaction similar in magnitude to nucleons, but under such conditions, the appearance of H particle would be significantly delayed beyond the NS central density. As a result, the pressure of NS matter containing H particles destines to decrease with increasing density, sooner or later.

The particle fractions as a function of the baryon number density  $n_b$  are displayed in Fig. 3. Upon the appearance of H particle, the fractions of all other types of particles, such as nucleons and leptons, immediately decrease. Our results are different from the behavior of another hexaquark  $d^*(2380)$  shown in Ref. [13], where the appearance of  $d^*(2380)$  leads to an increasing fraction of leptons. This is because  $d^*(2380)$  is positively charged, therefore, its appearance requires an increasing lepton fraction in order to maintain the charge neutrality. Consequently, the lepton degeneracy pressure contributes positively to the total pressure, resulting in a slower decrease in the pressure of NS matter due to the appearance of  $d^*(2380)$ , compared to that containing H particle. Since the H particle is electrically neutral, its presence results in a higher proportion of H particles as the density increases, which leads to a decrease in the fractions of neutrons and protons. The fraction of leptons decreases synchronously with the fraction of protons. With increasing density, the process of neutronization in NS can be considered as a decrease in the electron fraction. This situation is also applicable to deconfinement phase transitions. In this study, the appearance of the H particle promotes the reduction of electron number, thereby squeezing out the proportion of nucleons. The purely repulsive interaction  $(\chi_{\sigma H}, \chi_{\omega H}) = (0, 0.5)$  of H particles causes the fractions of other particles to decrease more rapidly (The curves depicting  $(\chi_{\sigma H}, \chi_{\omega H}) = (0, 0.5)$  terminate around 0.7-0.8 fm<sup>-3</sup> in panels a, b, and d due to

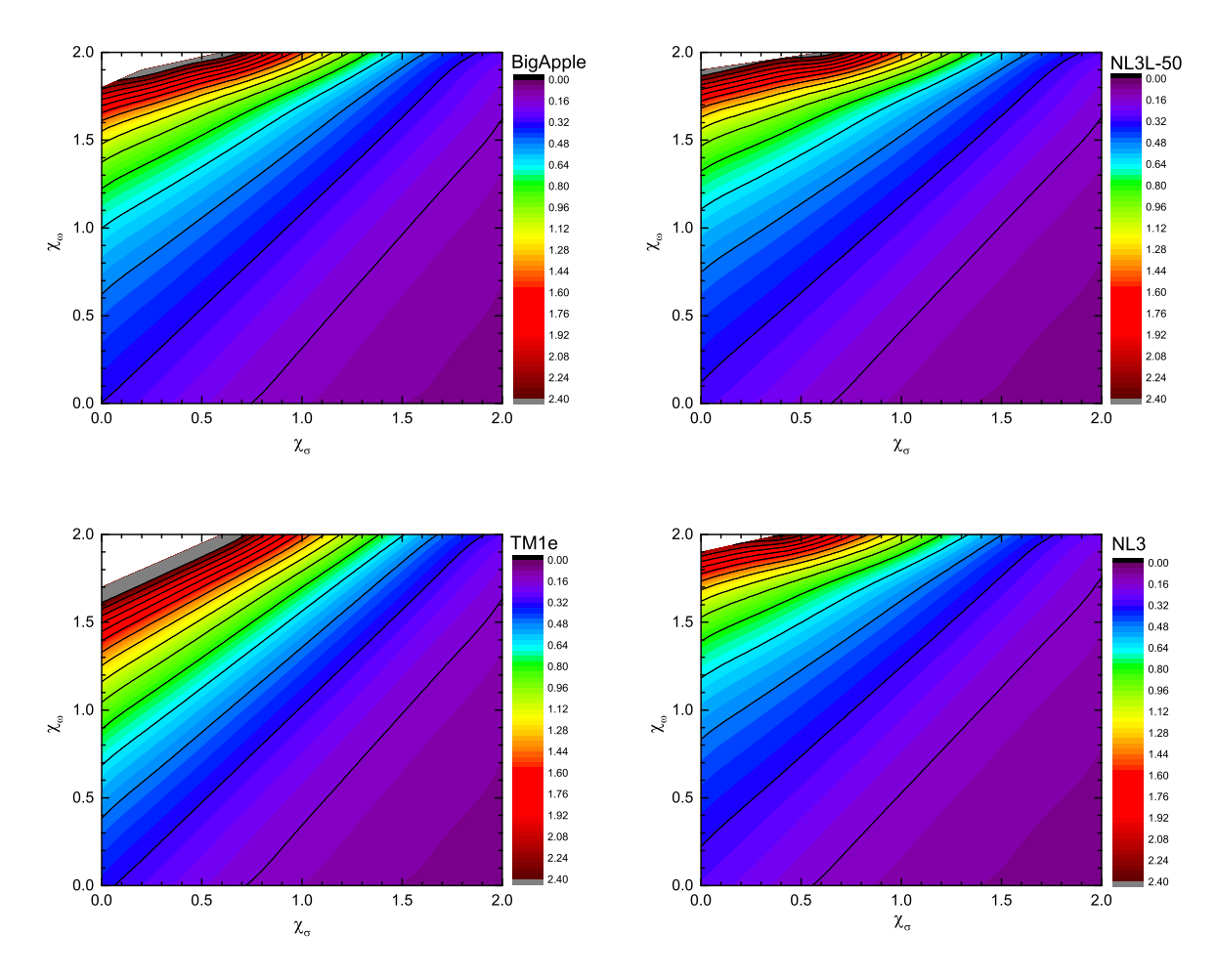


FIG. 1: Onset density (in unit of fm<sup>-3</sup>) of H particle in  $\beta$ -stable NS matter as a function of the dimensionless coupling  $\chi_{\sigma H}$  and  $\chi_{\omega H}$ .

the occurrence of collapse, see details in Fig. 4). Including attractive interaction  $(\chi_{\sigma H}, \chi_{\omega H}) = (0.5, 1)$  increases the fraction of H particles. The influence of different couplings on the onset of the H particle can be found in Fig. 1. In general, a total repulsive interaction delays the appearance of the H particle.

In Fig. 4, we present the pressures obtained using different RMF/RMFL models, considering various interactions of H particles. The interaction of H particles is assumed to be either purely repulsive with couplings  $(\chi_{\sigma H}, \chi_{\omega H}) = (0, 0.5), (0, 1)$  or totally repulsive with couplings  $(\chi_{\sigma H}, \chi_{\omega H}) = (0.5, 1), (1, 1.5)$ . For comparison, the non-interacting case  $(\chi_{\sigma H}, \chi_{\omega H}) = (0, 0)$  is also included. The condition of totally attractive interactions is not depicted here, as the immediate reduction in pressure does not support the stable existence of H particles (except part of NL3L-50 results in Fig. 2). The onset of H particle can also be observed in Fig. 1. Clearly, the system becomes unstable at high density under the conditions  $(\chi_{\sigma H}, \chi_{\omega H}) = (0, 0.5), (1, 1.5), (0, 1)$ . Other cases in Fig. 4 like  $(\chi_{\sigma H}, \chi_{\omega H}) = (0.5, 1)$  will also decrease at

very high density. If there is an increase in pressure following the appearance of the H particle, it could survive in NS matter at least for a range of density.

In Figs. 5 and 6, we display the mass-radius relations (left panel) and mass-central density relations (right panel) of NS predicted by using the EOSs utilized in Fig. 4. Additionally, several constraints derived from astrophysical observations are included in the figures. With  $(\chi_{\sigma H}, \chi_{\omega H}) = (0, 0.5)$ , the pressure does not decrease soon after the appearance of H particle (see Fig. 2), but the increase of the pressure does not strong enough to resist gravity and the star would collapse, which is similar as  $(\chi_{\sigma H}, \chi_{\omega H}) = (0,0)$  for NL3L-50. In the case of  $(\chi_{\sigma H}, \chi_{\omega H}) = (0,0)$  for Bigapple, TM1e and NL3, the pressure decreases soon after the appearance of H particle (see Fig. 2), so that it leads to the collapse of the star. Generally the introduction of new degrees of freedom, such as H particle in this work, always reduces the maximum mass of NS. Consequently, the results of mass and radius exhibit a clear deviation from the pure hadronic mass-radius line. For  $(\chi_{\sigma H}, \chi_{\omega H}) =$ 

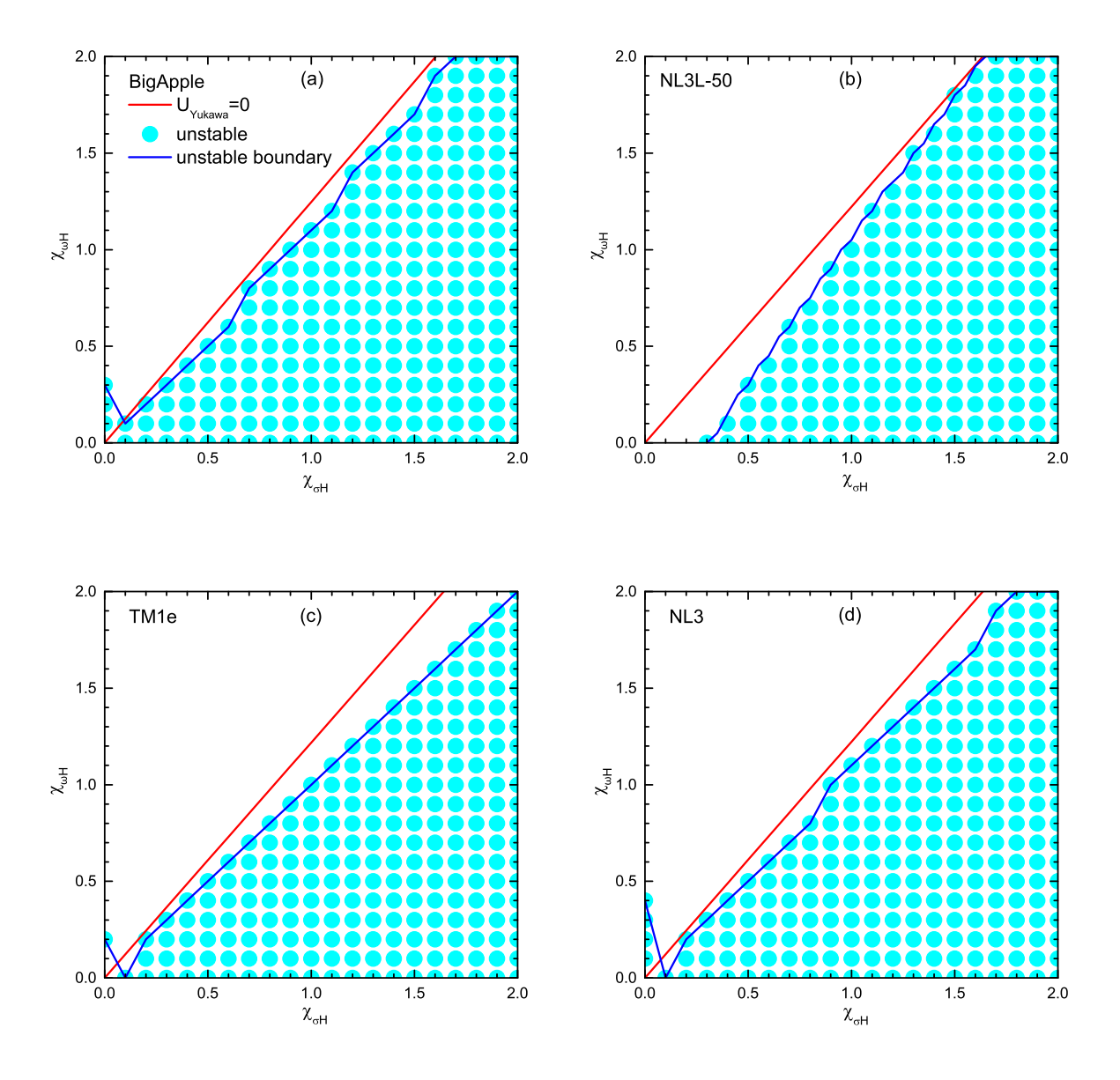


FIG. 2: The solid blue line shows the area boundary of the zone where H particle's appearance leads to decreasing pressure. The red line corresponds to the critical boundary where Yukawa potential equals zero.

(0.5, 1), (1, 1.5), (0, 1), the results align with the typical addition of new degrees of freedom, like hyperons. By employing stiff EOSs of BigApple and NL3L-50, these couplings satisfy the constraints from astrophysical observations. Meanwhile, with TM1e, only  $(\chi_{\sigma H}, \chi_{\omega H}) = (1, 1.5), (0, 1)$  fulfill the constraints. Notably, the couplings that adhere to the constraints do not exert an influence on the properties of a  $M = 1.4 M_{\odot}$  NS, because the H particle appears at higher density than its central density. In the case of no-interaction coupling  $(\chi_{\sigma H}, \chi_{\omega H}) = (0, 0)$ , the H particle could appear below the central density of  $1.4 M_{\odot}$ , but the star collapses soon thereafter. The results obtained from NL3 fail to satisfy many of the observed constraints, as indicated in Fig. 6,

where NL3 yields excessively large radii due to its large value of symmetry energy slope L.

### V. CONCLUSIONS

In this study, we investigated the possibility of H particle's existence in NS. We first calculated the mass of the H particle using the CMI model, which predicted a possible  $J^P=0^+$  particle with a mass of 2212.7 MeV. To describe NS matter, we employed the RMF/RMFL model with different parameter sets, namely BigApple, NL3L-50, TM1e, and NL3. Meanwhile, we explored the presence of the H particle in NS matter considering var-

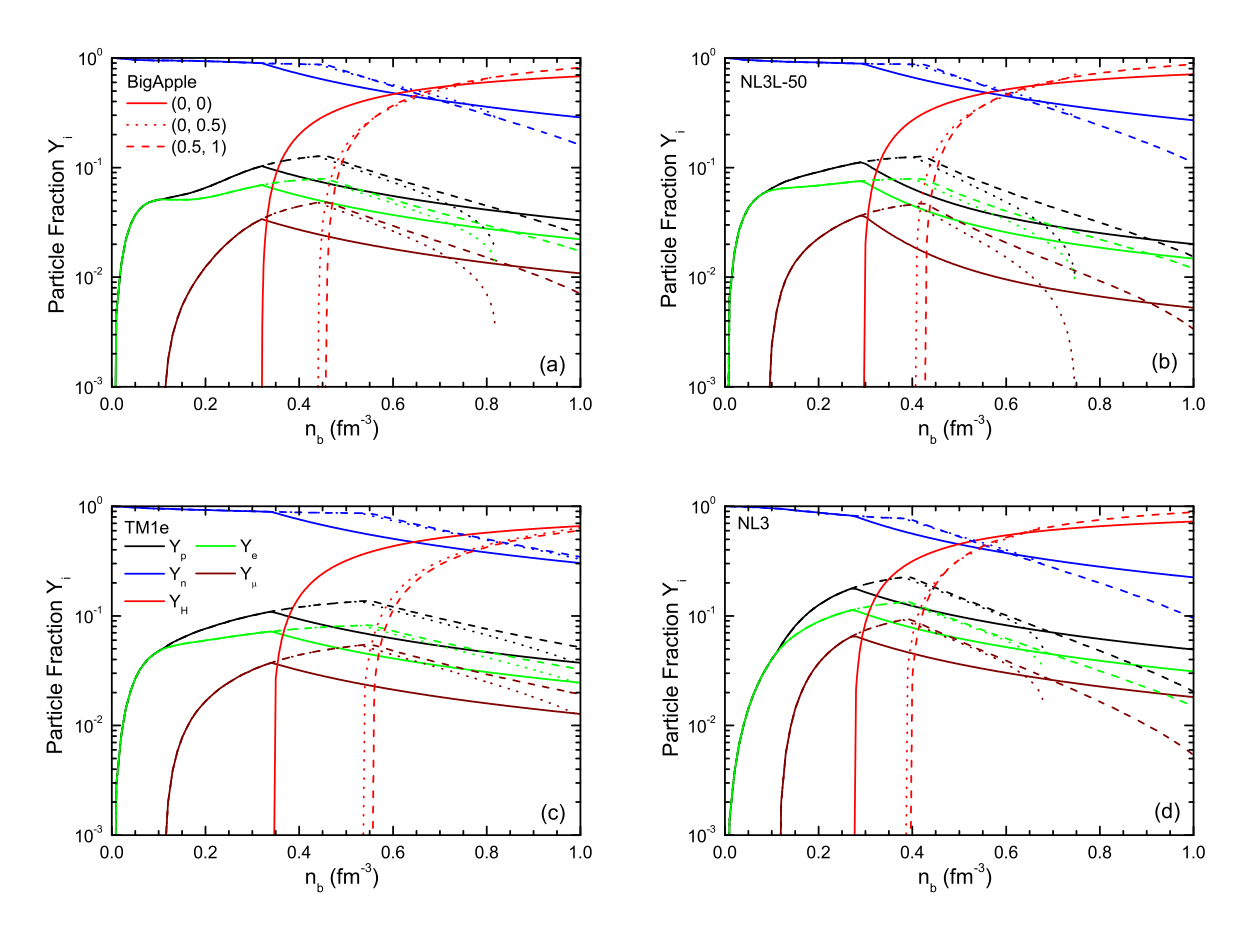


FIG. 3: Particle fractions as functions of the baryon number density  $n_b$  in different models. The three cases of H particle couplings used,  $(\chi_{\sigma H}, \chi_{\omega H})=(0, 0)$ , (0, 0.5), (0.5, 1), correspond to free H particle, purely repulsive interaction and both attractive and repulsive interaction.

ious choices of attractive and repulsive couplings ( $\chi_{\sigma H}$ and  $\chi_{\omega H}$ ). Our numerical results show some model dependence, but the behavior of H particle shares many commonalities. Except for the NL3L-50 parameter set, the existence of H particle with purely attractive interaction is not supported. In these cases, the appearance of H particle leads to the collapse of the NS into a black hole. Usually a total repulsive interaction is necessary to allow the existence of H particle in the core of NS, however, a small pure repulsive interaction is not sufficient to support the presence of the H particle in NS by using BigApple, TM1e and NL3. Interestingly, in the case of NL3L-50, even a slight total attractive interaction of H particle is permissible, since the pressure supplied by other particles can counterbalance the H particle's attractive potential, preventing the collapse of the NS. The presence of H particle generally reduce the maximum mass of NS. However, with a relatively large total repulsive interaction, the maximum mass can reach 2  $M_{\odot}$ , allowing for the possibility of H particle to exist in the core of the NS. On the other hand, a large enough total repulsive interaction can make the system more stable, but delays the appearance of H particle beyond the cen-

ter density of NS, which does not support its existence in NS.

Three types of collapse or instability are addressed in this study. The first one is the common NS collapse when the mass-radius line exceeds the maximum mass, where the strong interaction in normal NS matter consisting of  $npe\mu$  particles cannot resist the gravity. Such instability also occur when the H particles are taken into account with  $(\chi_{\sigma H}, \chi_{\omega H}) = (0, 1), (1, 1.5)$  and (0.5, 1). The second type was discussed in Fig. 2, where the presence of H particle causes an immediate decrease in the total pressure, which induces the stable  $npe\mu$  matter to be unstable  $npe\mu H$  matter with increasing density. These choices of  $(\chi_{\sigma H}, \chi_{\omega H})$  trigger the collapse after the H particle appears. The third one is the appearance of H particle does not immediately cause a drop in pressure. However, a decrease of the derivative of pressure with respect to density means that the interaction among particles becomes not strong enough to resist gravity and the star collapses. This was observed in cases  $(\chi_{\sigma H}, \chi_{\omega H}) = (0, 0)$ and (0, 0.5).

In summary, we conclude that from our analysis the presence of H particle within NS is plausible. To further

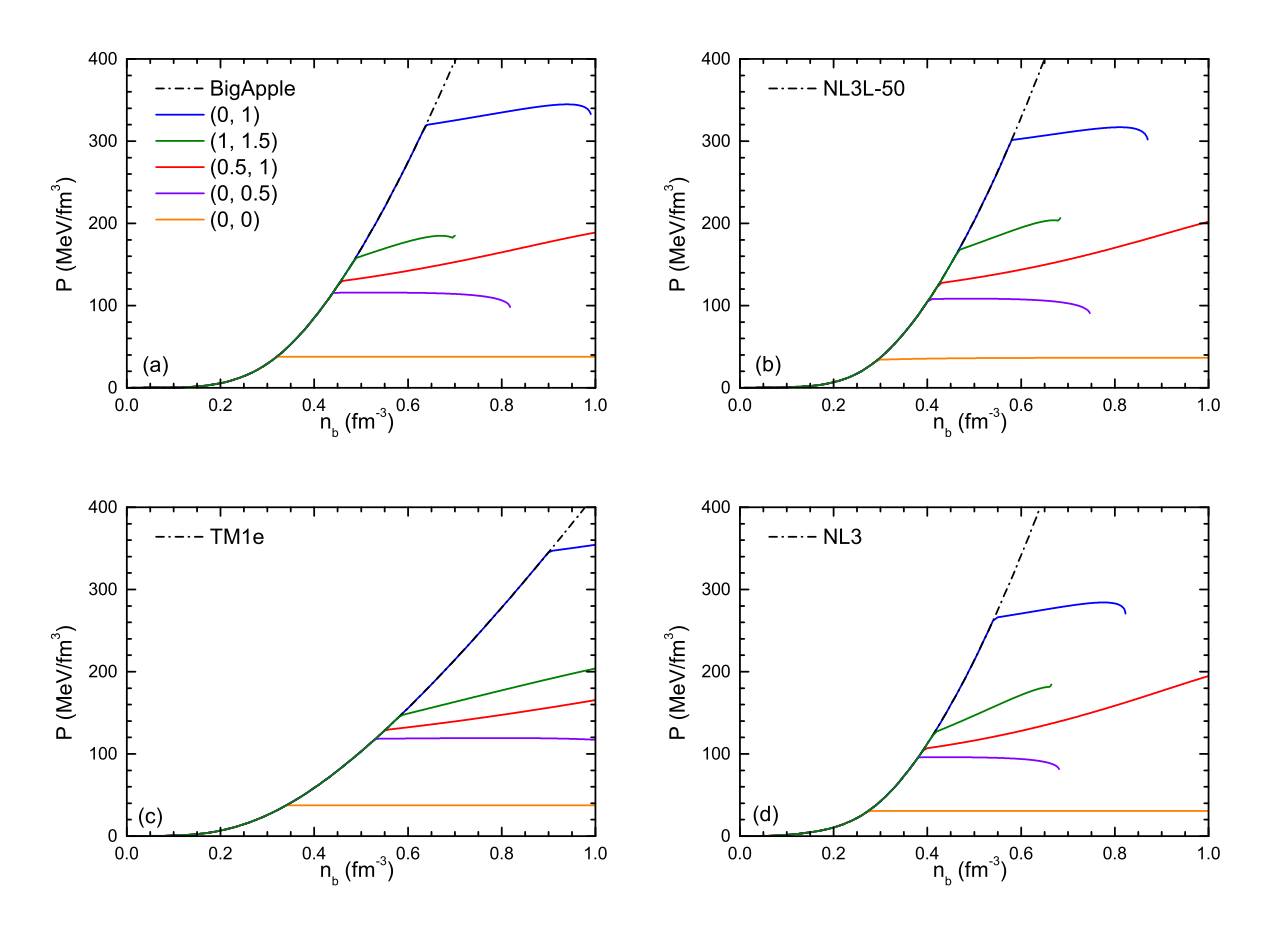


FIG. 4: Pressure P as a function of  $n_b$  with different couplings. The results using couplings  $(\chi_{\sigma H}, \chi_{\omega H}) = (0, 0), (0, 0.5), (0.5, 1), (1, 1.5), (0, 1)$  are shown. H particle admixed pressures split from those of pure hadronic matter when the H particles appear.

investigate the exact density at which the H particle appears and its fraction within NS, one possible approach is to use the quark-meson coupling (QMC) method [3, 56] to calculate the interaction potential, similar to the reappearance of hyperon potential. This would provide insights into the behavior of the H particle within NS. In the present work, we considered H particle as only non-nucleonic degree of freedom. If other degrees of freedom like hyperons,  $\Delta$ -isobar or  $d^*(2380)$  are taken into account, the results will change. However, due to the charge neutrality nature of NS, it is expected that these particles would not compete with the H particle in terms of their presence within NS. Further research is needed to explore these aspects in more detail.

# Acknowledgments

This work was supported in part by the National Natural Science Foundation of China under Grants No. 12305148 and No. 12175109, Hebei Natural Science Foundation No. A2023203055 and No. A202203026, and the Shandong Provincial Natural Science Founda-

tion, China under Grants No. ZR2023QA112.

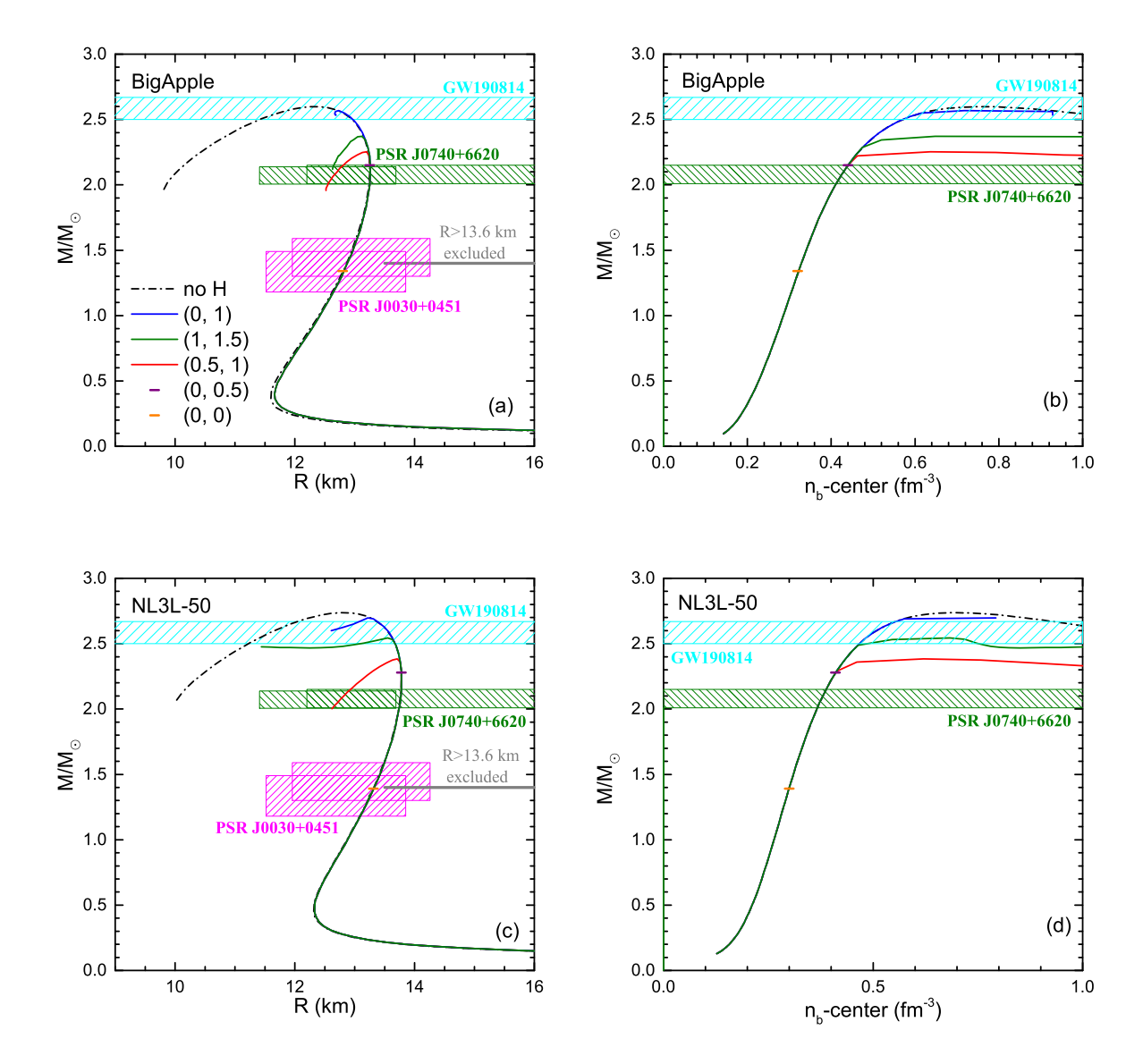


FIG. 5: Mass-radius relations and mass-central density relations for different models and couplings. The results of pure hadronic EOS (dash-dot lines) are compared with those including H particle for different couplings (same as Fig. 4). The shaded areas correspond to simultaneous measurements of the mass and radius range from NICER for PSR J0030+0451 [36, 37] and PSR J0740+6620, respectively [38, 39]. The hypothesis that the second component of GW190814 is a NS is also depicted [42]. The inferred radius constraint from GW170817 is shown by grey line [41].

<sup>[1]</sup> R. L. Jaffe, Phys. Rev. Lett. 38, 195, 617(E) (1977).

<sup>[2]</sup> F. Weber, M. Meixner, R. P. Negreiros, and M. Malheiro, Int. J. Mod. Phys. E 16, 1165-1180 (2007).

<sup>[3]</sup> J. Rikovska-Stone, P. A. M. Guichon, H. H. Matevosyan, A. W. Thomas Nucl. Phys. A 792, 341-369, (2007).

<sup>[4]</sup> P. K. Panda, D. P. Menezes, C. Providência, Phys. Rev. C 69, 025207 (2004).

<sup>[5]</sup> T. Katayama, K. Saito, Phys. Lett. B **747**, 43?47 (2015).

<sup>[6]</sup> J. J. Li, W. H. Long, and A. Sedrakian, Eur. Phys. J. A 54, 133 (2018).

<sup>[7]</sup> K. X. Huang, J. N. Hu, Y. Zhang & H. Shen, Nucl. Phys.

Rev. 39, 2 (2022).

<sup>[8]</sup> A. Drago, A. Lavagno, G. Pagliara, D. Pigato, Phys. Rev. C 90 065809 (2014).

<sup>[9]</sup> H. S. Sahoo, G. Mitra, R. Mishra, P.K. Panda, B.-A. Li, Phys. Rev. C 98, 045801 (2018).

<sup>[10]</sup> Z. Y. Zhu, A. Li, J. N. Hu, H. Sagawa, Phys. Rev. C 94 045803 (2016).

<sup>[11]</sup> J. J. Li, A. Sedrakian, F. Weber, Phys. Lett. B 810, 135812 (2020).

<sup>[12]</sup> A. R. Raduta, Phys. Lett. B 814 136070 (2021).

<sup>[13]</sup> A. Mantziris, A. Pastore, I. Vidaña, D. P. Watts, M.

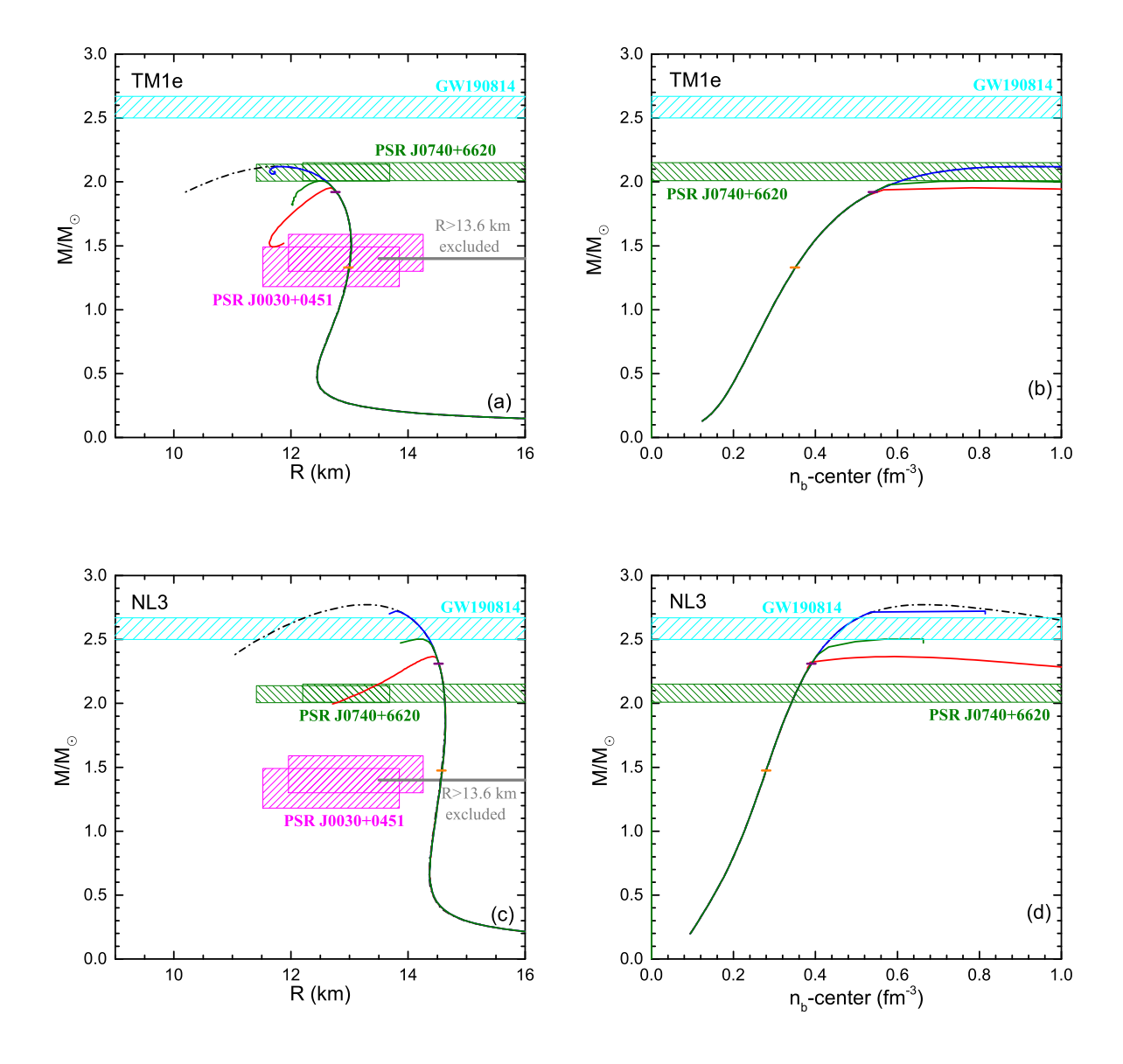


FIG. 6: Same as Fig. 5 but for TM1e and NL3.

Bashkanov, and A. M. Romero, A&A 638, A40 (2020).

- [14] A. Faessler, A. J. Buchmann, and M. I. Krivoruchenko, Phys. Lett. B 391, 255 (1997).
- [15] A. Faessler, A. J. Buchmann, and M. I. Krivoruchenko, Phys. Rev. C 56, 1576 (1997).
- [16] A. Faessler, A. Buchmann, M. Krivoruchenko, and B. Martemyanov, J. Phys. G, 24, 791 (1998).
- [17] N. K. Glendenning and J. Schaffner-Bielich, Phys. Rev. C 58, 1298 (1998).
- [18] N. K. Glendenning, Phys. Rep. 342, 393 (2001).
- [19] H. Heiselberg and M. Hjorth-Jensen, Phys. Rep. 328, 237 (2000).
- [20] F. Weber, Prog. Part. Nucl. Phys. 54, 193 (2005).
- [21] S. Benic, D. Blaschke, D. E. Alvarez-Castillo, T. Fischer and S. Typel, Astron. Astrophys. 577, A40 (2015)
- [22] K. Nakazato, K. Sumiyoshi, and S. Yamada, Phys. Rev. D 77, 103006 (2008).

- [23] X. H. Wu and H. Shen, Phys. Rev. C 99, 065802 (2019).
- [24] M. Ju, J. N. Hu, H. Shen, Astrophys. J. 923(2), 250 (2021).
- [25] İ. Vidaña, M. Bashkanov, D.P. Watts, A. Pastore, Phys. Lett. B 781, 112?116 (2018).
- [26] M. Bashkanov, S. Kay, D. Watts, et al., Phys. Lett. B 789, 7 (2019).
- [27] H. Kim, K. S. Kim, and M. Oka, Phys. Rev. D 102, 074023 (2020).
- [28] P. Adlarson, M. Bashkanov, H. Clement, et al., Phys. Rev. Lett. 112, 202301 (2014).
- [29] E. Witten, Phys. Rev. D 30, 272 (1984).
- [30] H. Liu, Y.-H. Yang, Y. Han, and P.-C. Chu, Phys. Rev. D 108, 034004 (2023).
- [31] E. Fonseca, H.T. Cromartie, T.T. Pennucci, et al., Astrophys. J. Lett. 915, L12 (2021).
- [32] H. T. Cromartie, E. Fonseca, S. M. Ransom, et al., Nat.

- Astron. 4, 72 (2020).
- [33] R. W. Romani, D. Kandel, A.V. Filippenko, T.G. Brink, W. Zheng, Astrophys. J. Lett. 934, L18 (2022).
- [34] Z. Arzoumanian et al., Astrophys. J. Suppl. 235, 37 (2018).
- [35] J. Antoniadis, P. C. C. Freire, N. Wex, et al., Sci. 340, 448 (2013).
- [36] T. E. Riley et al., Astrophys. J. Lett. 887, L21 (2019).
- [37] M. C. Miller et al., Astrophys. J. Lett. 887, L24 (2019).
- [38] T. E. Riley, A. L. Watts, P. S. Ray et al., Astrophys. J. Lett. 918, L27 (2021).
- [39] M. C. Miller, F. K. Lamb, A. J. Dittmann et al., Astrophys. J. Lett. 918, L28 (2021).
- [40] B. P. Abbott, et al.(The LIGO Scientific Collaboration and the Virgo Collaboration) Phys. Rev. Lett. 119, 161101 (2017).
- [41] E. Annala, T. Gorda, A. Kurkela, A. Vuorinen, Phys. Rev. Lett. 120, 172703 (2018).
- [42] R. Abbott et al. (LIGO Scientific and Virgo Collaborations), Astrophys. J. Lett. 896, L44 (2020).
- [43] Y. R. Liu, H. X. Chen, W. Chen, X. Liu and S. L. Zhu, Prog. Part. Nucl. Phys. 107, 237-320 (2019).
- [44] X. Z. Weng, X. L. Chen, W. Z. Deng and S. L. Zhu, Phys. Rev. D 100 no.1, 016014 (2019).
- [45] Z. Liu, H. T. An, Z. W. Liu and X. Liu, Chin. Phys. C

- 47 no.6, 063105 (2023).
- [46] H. T. An, K. Chen, Z. W. Liu and X. Liu, Phys. Rev. D 103 no.11, 114027 (2021).
- [47] W. Park, A. Park, S. Cho and S. H. Lee, Phys. Rev. D 95 no.5, 054027 (2017).
- [48] W. Park, A. Park and S. H. Lee, Phys. Rev. D 92 no.1, 014037 (2015).
- [49] H. T. An, K. Chen, Z. W. Liu and X. Liu, Phys. Rev. D 103 no.7, 074006 (2021).
- [50] F. Stancu and S. Pepin, Few Body Syst. 26, 113-133 (1999).
- [51] F. J. Fattoyev, C. J. Horowitz, J. Piekarewicz, and B. Reed, Phys. Rev. C 102, 065805 (2020).
- [52] X. H. Wu, S. S. Bao, H. Shen, R. X. Xu, Phys. Rev. C 104, 015802 (2021).
- [53] S. S. Bao, J. N. Hu, Z. W. Zhang, and H. Shen, Phys. Rev. C 90, 045802 (2014).
- [54] X. H. Wu, A. Ohnishi, and H. Shen, Phys. Rev. C 98, 065801 (2018).
- [55] G. A. Lalazissis, J. König and P. Ring, Phys. Rev. C 55, 540 (1997).
- [56] P. A. M. Guichon, J. R. Stone, A. W. Thomas, Prog. Part. Nucl. Phys. 100, 262 (2018).